NASA/TM—2016-219095

Temperature Dependence of Electrical Resistance of Woven Melt-Infiltrated SiC_f/SiC Ceramic Matrix Composites

Matthew P. Appleby
Glenn Research Center, Cleveland, Ohio

Gregory N. Morscher
The University of Akron, Akron, Ohio

Dongming Zhu
Glenn Research Center, Cleveland, Ohio

May 2016

NASA STI Program . . . in Profile

Since its founding, NASA has been dedicated to the advancement of aeronautics and space science. The NASA Scientific and Technical Information (STI) Program plays a key part in helping NASA maintain this important role.

The NASA STI Program operates under the auspices of the Agency Chief Information Officer. It collects, organizes, provides for archiving, and disseminates NASA's STI. The NASA STI Program provides access to the NASA Technical Report Server—Registered (NTRS Reg) and NASA Technical Report Server—Public (NTRS) thus providing one of the largest collections of aeronautical and space science STI in the world. Results are published in both non-NASA channels and by NASA in the NASA STI Report Series, which includes the following report types:

- TECHNICAL PUBLICATION. Reports of completed research or a major significant phase of research that present the results of NASA programs and include extensive data or theoretical analysis. Includes compilations of significant scientific and technical data and information deemed to be of continuing reference value. NASA counter-part of peer-reviewed formal professional papers, but has less stringent limitations on manuscript length and extent of graphic presentations.

- TECHNICAL MEMORANDUM. Scientific and technical findings that are preliminary or of specialized interest, e.g., "quick-release" reports, working papers, and bibliographies that contain minimal annotation. Does not contain extensive analysis.

- CONTRACTOR REPORT. Scientific and technical findings by NASA-sponsored contractors and grantees.

- CONFERENCE PUBLICATION. Collected papers from scientific and technical conferences, symposia, seminars, or other meetings sponsored or co-sponsored by NASA.

- SPECIAL PUBLICATION. Scientific, technical, or historical information from NASA programs, projects, and missions, often concerned with subjects having substantial public interest.

- TECHNICAL TRANSLATION. English-language translations of foreign scientific and technical material pertinent to NASA's mission.

For more information about the NASA STI program, see the following:

- Access the NASA STI program home page at http://www.sti.nasa.gov

- E-mail your question to help@sti.nasa.gov

- Fax your question to the NASA STI Information Desk at 757-864-6500

- Telephone the NASA STI Information Desk at 757-864-9658

- Write to:
  NASA STI Program
  Mail Stop 148
  NASA Langley Research Center
  Hampton, VA 23681-2199

NASA/TM—2016-219095

Temperature Dependence of Electrical Resistance of Woven Melt-Infiltrated SiC_f/SiC Ceramic Matrix Composites

Matthew P. Appleby
Glenn Research Center, Cleveland, Ohio

Gregory N. Morscher
The University of Akron, Akron, Ohio

Dongming Zhu
Glenn Research Center, Cleveland, Ohio

National Aeronautics and
Space Administration

Glenn Research Center
Cleveland, Ohio 44135

May 2016

Acknowledgments

This work was supported by the NASA Glenn Research Center, under the Gradual Student Researchers Grant No. NNX11AL03H, and also by the NASA Transformational Tools and Technologies Project. The authors would like to gratefully acknowledge Jon Mackey for his testing and technical support.

This work was sponsored by the Fundamental Aeronautics Program at the NASA Glenn Research Center.

Level of Review: This material has been technically reviewed by technical management.

Available from

NASA STI Program
Mail Stop 148
NASA Langley Research Center
Hampton, VA 23681-2199

National Technical Information Service
5285 Port Royal Road
Springfield, VA 22161
703-605-6000

This report is available in electronic form at http://www.sti.nasa.gov/ and http://ntrs.nasa.gov/

Temperature Dependence of Electrical Resistance of Woven Melt-Infiltrated SiC_f/SiC Ceramic Matrix Composites

Matthew P. Appleby*
National Aeronautics and Space Administration
Glenn Research Center
Cleveland, Ohio 44135

Gregory N. Morscher
The University of Akron
Akron, Ohio 44325

Dongming Zhu
National Aeronautics and Space Administration
Glenn Research Center
Cleveland, Ohio 44135

Abstract

Recent studies have successfully shown the use of electrical resistance measurements to monitor room temperature damage accumulation in SiC/SiC CMCs. In order to determine the feasibility of resistance monitoring at elevated temperatures, the present work investigates the temperature dependent electrical response of various MI-CVI SiC/SiC composites containing Hi-Nicalon Type S, Tyranno ZMI and SA reinforcing fibers. Test were conducted using a commercially available isothermal testing apparatus as well as a novel, laser-based heating approach developed to more accurately simulate thermomechanical testing of CMCs. Secondly, a post-test inspection technique is demonstrated to show the effect of high-temperature exposure on electrical properties. Analysis was performed to determine the respective contribution of the fiber and matrix to the overall composite conductivity at elevated temperatures. It was concluded that because the silicon-rich matrix material dominates the electrical response at high temperature, ER monitoring would continue to be a feasible method for monitoring stress dependent matrix cracking of melt-infiltrated SiC/SiC composites under high temperature mechanical testing conditions. Finally, the effect of thermal gradients generated during localized heating of tensile coupons on overall electrical response of the composite is determined.

Introduction

Due to their high temperature durability and strength, ceramic matrix composites (CMCs) are currently under development for implementation in aero and nuclear turbine hot-sections. Among the various CMC systems being investigated, silicon carbide (SiC) fiber-reinforced melt-infiltrated (MI) SiC matrix composites have been shown to possess increased high temperature capabilities up to 1315 °C (Refs. 1 to 3). These properties are attributed to the increased densification of MI composites over competing SiC_f/SiC CMC processing methods, such as polymer infiltration and pyrolysis (PIP) and chemical vapor infiltration (CVI). The decrease in matrix porosity helps to decrease paths for environmental attack on the reinforcing fibers as well as increasing the load carrying capability of the matrix.

If CMCs are to be used in structural applications, it becomes crucial to investigate and understand the critical damage mechanisms associated with their proposed operating environments. Due to the semiconducting nature of their constituents, electrical resistance (ER) measurements have been shown to be effective in sensing damage in several SiC_f/SiC CMC systems. Recent work has been performed using

*The University of Akron intern.

electrical resistance monitoring to successfully detect damage accumulation, in the form of transverse matrix cracking, in both CVI (Ref. 4) and MI-CVI SiC_f/SiC CMCs (Ref. 5) under room temperature tensile loading. Morscher et al. were able to show that the increase in stress-dependent matrix crack accumulation to rupture increases the ER of the test coupon by hundreds of percent. The work also showed that when performing successive unload/reload cycles, a residual increase in ER at complete unload was related to the increased strain at zero stress caused by matrix cracking and associated matrix/fiber debonding (Ref. 5). This finding leads to the possibility of using ER not only as an in-situ monitoring technique, but also as a post-test inspection technique as well.

However, because these CMC materials are intended to be used at elevated temperatures, understanding the high temperature damage mechanisms and stress-rupture properties becomes the critical focus. Recent investigations have been performed using ER to characterize the high temperature creep properties of MI composites under both furnace-heated (quasi-isothermal) and laser-heated high heat-flux (thermal gradient) conditions (Ref. 6). While this work points out an obvious correlation between strain and ER increase, it also reveals the fact that the electrical response under these conditions can be quite convoluted and is not entirely understood. That is, when performing thermomechanical testing on SiC_f/SiC CMCs in oxidizing environments there are several potential factors that can influence ER response. Therefore, if ER is to be used for health monitoring, a systematic approach must be taken to understand the contributions of thermal and mechanical loading as well as environmental effects.

The present work attempts to describe the electrical response of MI-CVI SiC_f/SiC composites, and the contribution from their various constituents, under thermal loading conditions only. Some limited literature data does exist on the temperature dependence of electrical resistivity for various polycrystalline SiC fiber types which extends into the temperature range of interest (Ref. 7), as well as some CVI-SiC_f/SiC composite systems (Refs. 8 and 17). However, the ER response of MI composites to thermal loading is presumed to be significantly different due to the nature of the siliconized silicon carbide (Si-SiC) matrix material created during the molten silicon infiltration process. The relative high volume fraction of free silicon (Si) left in the matrix after processing (5 to 15 percent), will tend to make the matrix material considerably more conductive than that of a purely CVI matrix. Some interesting work has been performed characterizing the temperature dependent ER response of Si-SiC with various dopant types and concentrations (Ref. 9). The experimental data illustrates the significant contribution of the excess silicon to the overall electrical response of the system. Therefore, because the electrical resistivity is dependent on both temperature and microstructure, in order to expand ER monitoring to high temperature thermomechanical testing of MI SiC_f/SiC CMCs it first becomes necessary to characterize the temperature dependent response of these composites and their constituents.

This paper describes two separate experimental techniques for measuring the temperature dependent electrical resistivity of silicon melt-infiltrated SiC_f/SiC composite systems of various reinforcing fiber type: Hi-Nicalon Type S, Tyranno SA and ZMI. The second of which is a novel laser-based heating technique that utilizes standard tensile bar specimens used in mechanical testing. The physical mechanisms that dominate the electrical response in different temperature regions are generalized, and when available experimental data from literature is used in order to understand the contribution of the different composite constituents to electrical conduction. To demonstrate this, a simple parallel resistance model is presented that can be used in order to generalize the contribution of each constituent to the overall electrical behavior of the composite system. The results of this model confirm that even at elevated temperatures the electrical current flow through the composite is dominated by the matrix material. Since this is the main operating principle of ER monitoring of room temperature damage, this work confirms the applicability of extending ER measurements for elevated temperature damage characterization. Finally, as the experimental setup utilized in the high temperature laser-heating approach results in the generation of a thermal gradient across the measured length of the sample, the effect of the thermal gradient on the overall electrical response of the material is discussed. A model composed of a series resistance model of temperature dependent elements is presented and compared to experimentally measured ER data.

Experimental Materials and Procedure

All of the composites tested in this study consisted of 8 plies of balanced 0°/90°, 5 harness-satin woven fiber preforms of either: Hi-Nicalon Type S, Tyranno SA or ZMI reinforcing fibers. Using a chemical vapor deposition process the fiber preforms were then coated in a boron nitride (BN) interphase, followed by a layer of CVI SiC, and final densification by a slurry cast molten silicon melt-infiltration process (creating a Si-SiC matrix). The samples consisting of Hi-Nicalon Type S (HNS) fibers were manufactured by Hyper-Therm HTC, Inc. (Huntington Beach, CA, now part of Rolls-Royce), while the composites containing the Tyranno SA and ZMI fibers were manufactured by the Goodrich Corporation (Brecksville, Ohio, now part of United Technologies). The study of various fiber types and material manufacturers provides valuable insight into potential variations in electrical response due to differences in both constituent content and matrix microstructure.

Two separate experimental techniques were utilized to characterize the temperature dependent electrical response of the CMCs mentioned above. The first method involved the use of a commercially available ULVAC-ZEM3 unit (Ref. 10). The ZEM3 is a popular instrument in the field of thermoelectrics which uses a four-point probe method to measure the electrical resistance of a small test sample. In a four point probe method a constant electrical current is applied to the ends of a specimen via two outer electrodes, while two inner leads are used to measure the voltage drop caused by the resistivity of the material. The entire test-sample is heated in a low-pressure helium environment by an infrared gold image heating furnace. Figure 1 shows an image of the ZEM3 unit with a close-up of a typical specimen and the ER measurement configuration (all of which is housed within the furnace). The ZEM3 accommodates only small prismatic samples (6 to 22 mm in height), and is limited in its heating capabilities to approximately 900 °C (below the desired usage temperature for many MI-SiC_f/SiC CMC structural applications).

Details on the physical and geometrical properties of the CMC test samples measured using the ZEM3 can be found in Table 1. For all of the test specimens in this study the fiber volume fraction in the longitudinal direction, v_{f_0}, has been determined by dividing the cross-sectional area of the test coupon by the fiber area in the longitudinal direction. The fiber area can be estimated by multiplying the area of a single fiber by the number of fibers in a tow, number of tows per ply and number of plies in the lay-up (Ref. 11).

In order to overcome the sample geometry and temperature limitations of the ZEM3 unit, a second experimental technique was developed by the authors and used to determine the high temperature electrical properties of these CMC systems. This technique utilizes a 3.5 kW CO_2 laser to heat the front side of a 44 mm (1.75 in.) gage-section of a standard 152 mm (6 in.) tensile bar specimen (considerably larger than the samples that can be accommodated in the ZEM3 unit). Figure 2 shows a schematic of the laser-based heating setup with integrated ER measurement. This laser setup was specifically developed to demonstrate the capabilities of using ER measurements to monitor CMC tensile coupons up to their maximum operating temperatures. Therefore, this unique setup provides a useful temperature-dependent database as well as insight into the capability of utilizing ER monitoring for future characterization of CMCs under thermomechanical loading conditions. Table 1 outlines some of the relevant properties of the test specimens used in this laser-heating technique.

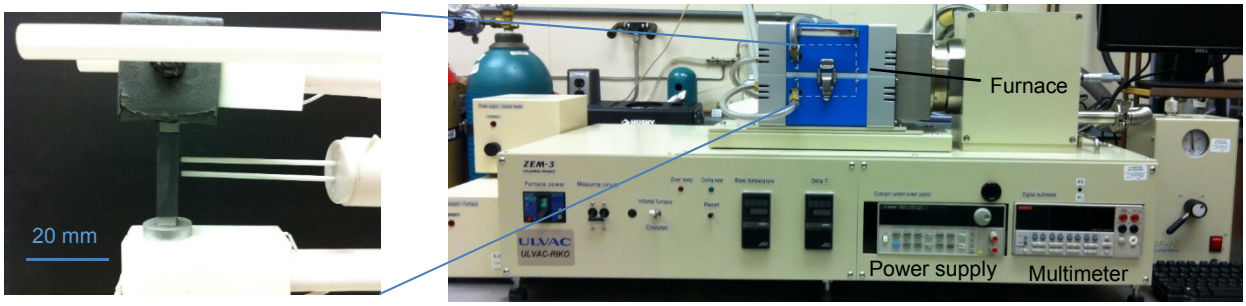

Figure 1.—ULVAC ZEM3 unit used for low/intermediate-temperature, isothermal characterization of SiC_f/SiC specimens. On the left is a close-up showing specimen and four-point probe configuration (note: entire specimen housed within furnace).

TABLE 1.—PHYSICAL AND GEOMETRICAL PROPERTIES OF TESTED SPECIMENS; SEPARATED BY FIBER TYPE AND TEST METHOD (i.e., ZEM3 OR LASER-BASED TESTING APPROACH)

	Cross-section[a] (mm × mm)	Average fiber radius (μm)	Fiber volume fraction (v_{f_0})
ZEM3 samples			
ZMI	4.00×4.19	5.5	0.1395
SA	2.80×2.15	5	0.1657
HNS	4.10×2.20	6	0.1478
Laser samples			
ZMI	10.05×4.12	5.5	0.1395
SA	10.06×2.11	5	0.1657
HNS	12.64×2.17	6	0.1476

[a]Dimensions refer to average gage width and thickness

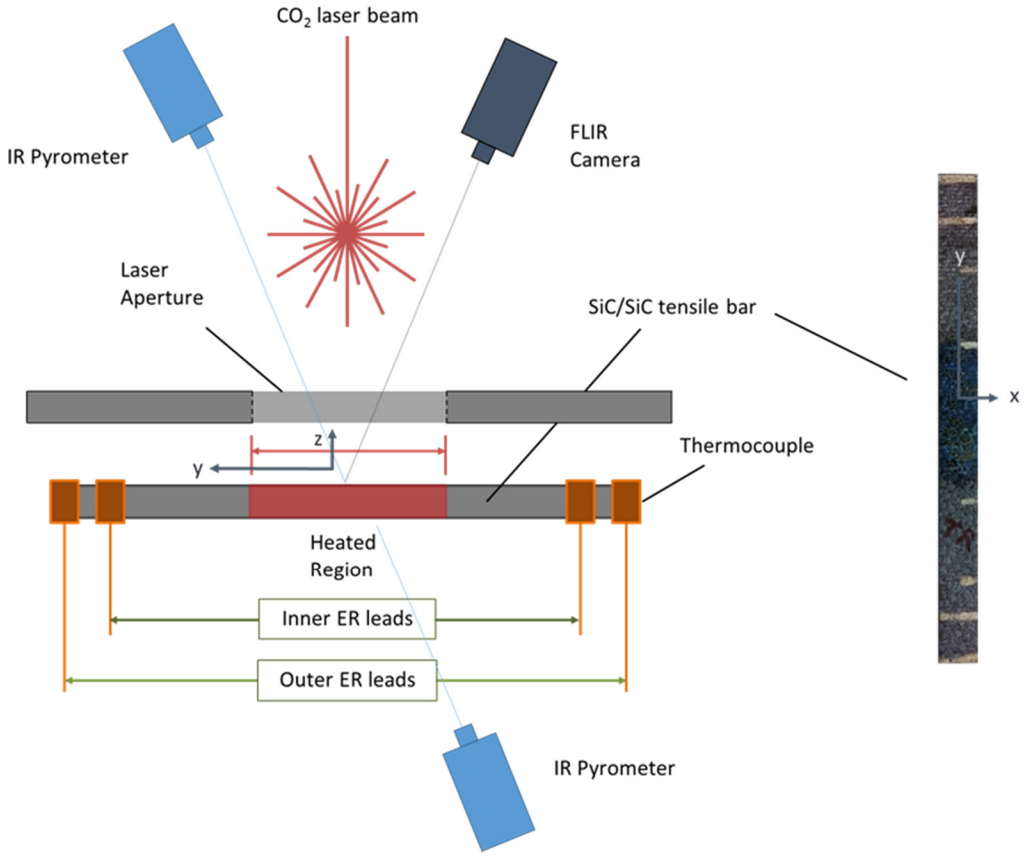

Figure 2.—Schematic of laser-based heating apparatus used for characterization of high-temperature electrical properties of SiC_f/SiC CMC tensile coupons.

The samples containing the Tyranno fibers had been machined into dog-bone specimens (approximate tab and gage widths of 12.7 and 10 mm, respectively), while the test specimen containing the HNS fibers was a straight sided bar (i.e., no variable cross section). A steel aperture plate containing a 44 mm (1.75 in.) diameter circular opening is used to assure a consistent laser-heated area, and the surface temperature of the hot-zone was monitored using an IRCON Modline 5 Series infrared pyrometer and FLIR thermal imaging system. This setup is capable of delivering a very stable beam profile, leading to a near constant temperature in the heated region (Ref. 12). The electrical resistance of the test specimen is monitored using an Agilent 34420A digital multimeter utilizing a four-point probe method. To avoid damage to the ER system caused by the high temperatures in the heated area, the outer ER electrodes are attached at the specimen ends and the inner electrodes attached at 15 mm from the specimen ends

(resulting in an inner probe separation distance of approximately 122 mm). Because the specimens are relatively thin, the surface heating generates a negligible through thickness thermal gradient. However, because only the gage section of the sample is heated, a longitudinal thermal gradient is generated from the edge of the heated region to the specimen end. Implications of the resulting thermal gradient on the sample response are discussed in the proceeding sections.

Results and Discussion

Room Temperature Resistivity

The as-produced room temperature electrical resistivity values for the specimens used in this study are listed in Table 2. The volumetric electrical resistivity, ρ, was calculated from the equation:

$$\rho = \frac{RA}{l} \tag{1}$$

where R is the electrical resistance determined from the four-point probe method described above, l is the inner probe distance and A is the average cross-sectional area (listed in Table 1) of the sample. The results of these measurements yield some interesting trends. First, the resistivity of the much larger (laser-heated) samples are considerably higher than the ZEM3 test specimens. While this is potentially coincidental, there is the possibility of size effects produced by an insulating effect at the grain boundaries of the constituents (especially the small grain size fibers (Ref. 13). That is, assuming a constant grain size between samples of different lengths, a smaller sample would contain less grain boundaries and hence a lower resistivity. A similar size effect could be caused by porosity such that, the electrical resistance of a smaller sample is going to be much more sensitive to porosity than that of a larger sample. Furthermore, it has been shown that the electrical resistivity measured via the ZEM3 unit contains an uncertainty of ±7 percent across any temperature measurement (Ref. 27). However, by far the most dominate mechanism controlling differences in sample resistivity is likely the consequence of processing variations. Though they may contain the same fiber types, the samples used for each type of test were from different processing batches (i.e., from separately produced CMC panels). The difference in free silicon content in the reaction bonded Si-SiC matrix resulting from the MI process could be significant, which due to the high electrical conductivity of silicon at room temperature (many orders of magnitude higher than SiC), would result in a considerable batch-variation effect on composite resistivity. This can lead to the considerable differences between different panels of the same composite architecture. However, a much less significant variation is seen when comparing the ER of each sample used in this study to other specimens machined from the same CMC panel. The room temperature resistivity of the samples tested are listed in Table 2.

To determine an average panel resistivity, the resistivity of a number of tensile specimens taken from the same panel as the test specimen were averaged in order to define a nominal panel resistivity. This average is then compared to the resistivity in each sample (Table 2). Note that the table lists: the average panel resistivity calculated, the number of specimens used to determine this average, and the corresponding scatter in measured values. In general, the resistivity of each sample is in good agreement with its respective nominal panel value.

TABLE 2.—ROOM TEMPERATURE ELECTRICAL RESISTIVITY (OHM-MM) OF SPECIMENS, AND CORRESPONDING AVERAGE PANEL RESISTIVITY

	ZEM3	Avg. [# of specimens] (scatter)	Laser	Avg. [# of specimens] (scatter)
Tyranno ZMI	0.667	0.545 [3] (+0.056/–0.083)	1.361	1.449 [3] (+0.208/–0.088)
Hi-Nicalon Type S	0.397	0.300 [3] (+0.097/–0.070)	0.931	0.909 [3] (+0.123/–0.117)
Tyranno SA	0.357	0.313 [6] (+0.078/–0.076)	0.649	1.043 [7] (+0.468/–0.393)

To further investigate the scattering in ER within a panel, discrete measurements along the length of the larger samples can be taken to illustrate the order of anisotropy. For example, Figure 3 shows room temperature ER values of the pre-tested, as-produced (pristine) sample, calculated for small increments along the length (± distance from the center of the sample) of the HNS-reinforced tensile specimen used in the laser-based heating test. The figure shows that there is a similar variation in ER within a sample as variation between samples in the same panel. This supports the previous conclusion that, while there is likely to be considerable batch-variation between CMC panels, the resistivity within a panel is considerably more uniform. Another interesting trend seen in the room temperature ER values listed in Table 2 is the consistency between sample types (ZEM3/laser) in terms of reinforcing fiber. That is, for both sets of samples the CMC resistivity is highest in the ZMI reinforced system and lowest in the SA. This trend seems to be consistent with that of recorded fiber resistivity that list these fibers in order of most-to-least resistive as: ZMI, HNS and finally SA (Refs. 9 and 14). This suggests to some extent the possible contribution of the fiber resistivity to the overall room temperature composite electrical response. However, it is difficult to determine the significance of fiber contribution since (as previously mentioned) the room temperature composite resistivity is largely dominated by the volume of Si in the MI matrix material. Finally, the values of room temperature ER measured post laser-heating indicate an interesting phenomenon resulting from the high temperature heat treatment of the CMC samples. In all cases, the effect of heat treatment on the specimens was to permanently increase the room temperature electrical conductivity (decrease resistivity) of the material. The ER values of the laser-heated samples decreased from the values listed in Table 2 (1.361, 0.931, 0.649 ohm-mm) to 1.263, 0.846, and 0.608 ohm-mm for the ZMI, HNS and SA samples respectively. Similar behavior was not evident however in the ZEM3 tested samples, presumably due to the lower maximum test temperatures to which they were exposed. To further investigate the effect of high temperature exposure on the electrical properties of the laser-heated samples, post-heating room temperature ER measurements were taken at the same locations as the pre-test measurements. Figure 3 shows the variation along the length of the HNS-reinforced tensile bar after being tested via the laser-heating technique.

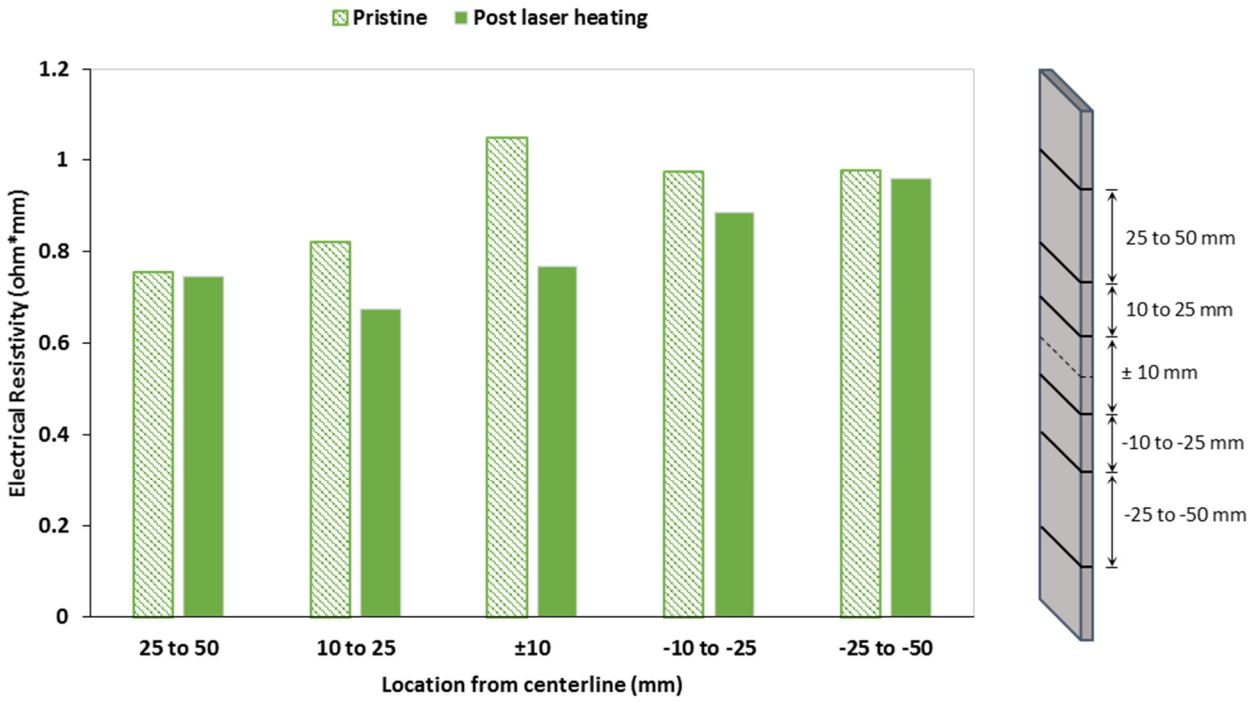

Figure 3.—Room temperature Electrical Resistivity measured from the centerline of the Hi-Nicalon Type S laser-heated sample, performed before heating (Pristine) and Post laser-heating. Note: the heated region of the composite specimen is approximately ±22 mm.

It is clear that the heated area of the sample saw the most significant residual increase is room temperature electrical conductivity, while the area outside the heated zone (±25 to 50 mm) saw only a negligible change. It is therefore concluded that exposure to high temperatures (>1000 °C) effectively changes the microstructure of the composite, resulting in a residual increase is room temperature conductivity. The electrical resistivity of semiconductors like SiC are controlled by various microstructural attributes including: the concentration and type of chemical impurities (dopants) within the material and at the grain boundaries, as well at the grain boundaries themselves (Ref. 19). Heat treatment of bulk SiC can precipitate these impurities, greatly changing the electrical properties of the material. Also, heat treatment of fine grained polycrystalline SiC fibers has been shown to lead to grain coarsening (grain growth) leading to a decreased number of grain boundaries (Refs. 13 and 21). Fewer grain boundaries leads to a lower barrier to electron movement and in turn an increase in electrical conductivity. An additional mechanism aiding in increasing conductivity is the possibility that high-temperature exposure decreases the residual thermal stresses within the matrix that were developed by cooling the material from processing temperature. This decrease in residual thermal stress could have a pressure effect on the free silicon within the Si-SiC matrix that results in an increase is conductivity. While it is evident that heating MI-CVI SiC_f/SiC composites to elevated temperatures increases their room temperature electrical conductivity, the mechanism that is most significant to the residual change observed in these materials is not known at this time. Looking ahead to applications in CMC damage characterization, the technique demonstrated in Figure 3 could be adopted to quantify post-test mechanical damage of CMCs by looking at the residual increase in ER at room temperature. This would be particularly helpful in identifying areas of increased localized damage associated with stress concentrations and local strain fields. Note that if this technique is being used for inspection following high-temperature mechanical testing, care must be taken to recognize the competing mechanism of conductivity increase due to high temperature exposure and increased resistivity due to accumulated composite damage.

Temperature Dependence of Electrical Resistivity

When considering the temperature dependent response of complex semiconductor materials like MI-CVI SiC_f/SiC CMCs, it is first important to consider the mechanisms controlling electron transport in semiconductor materials in general. Therefore, in terms of transport mechanics, electrical resistivity ρ can be expressed as the following:

$$\rho = \frac{1}{\sigma} \approx {}^{1}/_{ne\mu} \tag{2}$$

where the electrical response of the semiconductor is governed by the temperature dependencies of both the carrier concentration n and mobility μ, and where the electron charge e is considered a physical constant that does not depend on temperature. In terms of energy band theory, for an intrinsic semiconductor (i.e., a material that does not contain any charge donor or acceptor impurities/dopants) electrical conductivity is dictated purely by the number of electrons shifted from the valence to the conduction band. As temperature T increases the number of electrons excited to the conduction band increases, leaving a proportional number of holes/vacancies in the valence band. The intrinsic carrier concentration has been shown to be proportional to $T^{3/2}exp(-E_g/2kT)$, where E_g is the semiconductor band gap energy (the activation energy required to move an electron to the conductive band). Since intrinsic materials are free from any dopant atoms there is no effect of impurity scattering of electrons only thermally induced lattice scattering, resulting in electron and hole mobilities proportional to $T^{-3/2}$. The temperature dependencies of carrier concentration and mobility therefore result in an electrical resistivity controlled by an exponential relationship to the energy band gap $exp(E_g/2kT)$ (Ref. 20). The natural log of resistivity versus the reciprocal of absolute temperature plots are therefore often used to represent electrical data since such plots are indicative of the energy distribution of charge carriers in relation to thermally induced excitations.

The inclusion of small amounts of impurity atoms to a semiconductor can greatly affect the electrical properties. The temperature dependence of electron transport of extrinsic semiconductors (i.e., semiconductors containing impurity atoms) demonstrate a slightly more complicated behavior than pure semiconductor materials. In the temperature range corresponding to the extrinsic or saturation region, the carrier concentration is approximately equal to the impurity concentration (dopant density) thereby making carrier concentration effectively independent of temperature. Also, for low and moderate impurity concentrations, lattice scattering dominates and electron mobility decreases with temperature as $T^{-3/2}$. Therefore, due to the inverse proportionally of resistivity to mobility (Eq. (2)), materials at moderate dopant levels and temperatures will show an increasing resistivity with temperature. Resistivity will continue to increase with temperature until a transition temperature is reached at which carrier concentration begins increasing due to the significant number of bonds being ruptured at high temperature. The semiconductor then behaves essentially as an intrinsic material and resistivity decreases (conductivity increases) and follows the intrinsic curve. Increasing of the dopant concentration (number of conductive impurities) will effectively decrease the resistivity of the material, thereby shifting the $ln(\rho)$ versus inverse absolute temperature curve down the resistivity axis and move the onset of the intrinsic behavior to a higher temperature. That is, an increased number of bonds are required to be broken in order to increase the number of charge carriers to overcome the large number of dopant atoms. If dopant concentration is very high the effect of impurity scattering increases and at some dopant level will cancel out the effect of lattice scattering, making carrier mobility completely temperature independent. If the material is in the extrinsic temperature region where carrier concentration is also temperature independent, resistivity becomes effectively insensitive to temperature. Hence, heavily doped semiconductors show very little temperature dependence of electrical resistivity.

The electrical resistivity of MI-CVI SiC_f/SiC CMCs containing various fiber types was investigated up to approximately 900 and 1300 °C using a commercially available ZEM3 unit and novel laser-heating technique respectively. The results of the testing are shown in Figure 4. As with typical semiconductor materials, the initial increase in resistivity with temperature is the result of a reduction in carrier mobility caused by the lattice scattering of valence electrons. For these materials, this behavior appears to change

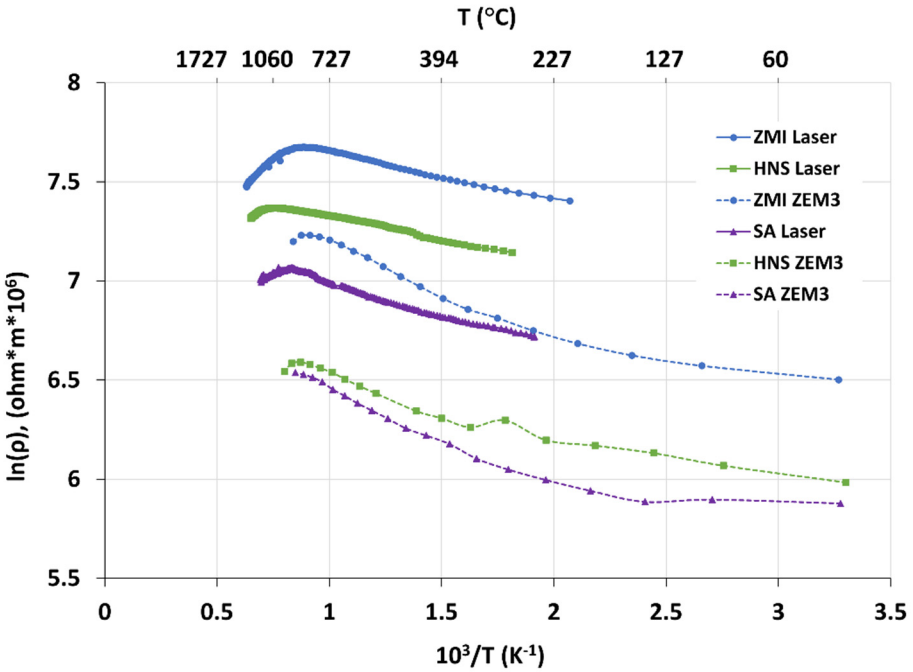

Figure 4.—Temperature dependent electrical response of MI-CVI SiC_f/SiC samples tested using the ZEM3 and laser-based heating technique, respectively.

at temperatures ranging from 900 to 1100 °C (depending on the composite microstructure and testing type) when presumably the increase in carrier concentration becomes more dominant and the samples start to become increasingly more conductive with temperature.

While all of the samples show trends of this nature, there are apparent differences in activation energies and transition temperatures caused by microstructural differences between specimens. It could therefore be possible to quantify differences in material microstructure based on their individual material response.

Isothermal Behavior and Parallel Constituent Model

If electrical resistance monitoring is to be extended for use in elevated temperature mechanical testing, it is critical that the contribution of each composite constituent at high temperature is well understood in order to correlate observed changes in ER with specific damage mechanisms. Therefore, if the composite is considered as two separate and continuous phases of: (1) fibers in the longitudinal direction v_{f_0}, and (2) an "effective" matrix material m_{eff} consisting of the fiber/matrix BN interphase, CVI SiC matrix, Si-SiC matrix, and transverse fiber tows (i.e., everything that is not fibers in the longitudinal direction), it is possible to model the composite as a parallel circuit in order to determine the contribution of each constituent phases to the overall electrical conductivity. This parallel circuit model should be a reasonable assumption since both of the assigned phases forms a continuous material throughout the composite. When parallel processes of electrical conduction exist, the total conductivity is the sum of the individual contributions. Therefore, the route with the highest conductivity dominates the conductivity of the system. With respect to resistivity, we can express this parallel circuit in terms of the reciprocal resistivity of each phase and their respective volume fractions. Using the known fiber resistivity and measured composite resistivity it is therefore possible to calculate the contribution of the effective matrix material.

$$v_{f_0} + v_{m\,eff} = 1 \tag{3}$$

$$\sigma_c = v_{f_0}\sigma_f + v_{m\,eff}\sigma_{m\,eff} \tag{4}$$

$$\sigma_{m\,eff} = \frac{\sigma_c - v_{f_0}\sigma_f}{1 - v_{f_0}} \tag{5}$$

$$\frac{1}{\rho_c} = \frac{v_{f_0}}{\rho_f} + \frac{v_{m\,eff}}{\rho_{m\,eff}} \tag{6}$$

$$\rho_{m\,eff} = \left(1 - v_{f_0}\right)\left(\frac{1}{\rho_c} - \frac{v_{f_0}}{\rho_f}\right)^{-1} \tag{7}$$

The parallel circuit assumption represented in Equation (6) shows that the reciprocal of the composite resistivity is the weighted average of the reciprocal of the constituents, where the weights following a rule of mixtures assumption representing the respective volume fractions of the fibers v_{f_0} and effective matrix $v_{m\,eff}$. To illustrate the use of this model to determine the temperature dependence of each composite phase (i.e., fibers and effective matrix), Figure 5 compares the calculated effective matrix conductivity $\sigma_{m\,eff}$ for the (a) HNS and (b) SA reinforced composites using the isothermal ZEM3 data and the fiber conductivity curves reported in Scholz et al. (Ref. 7).

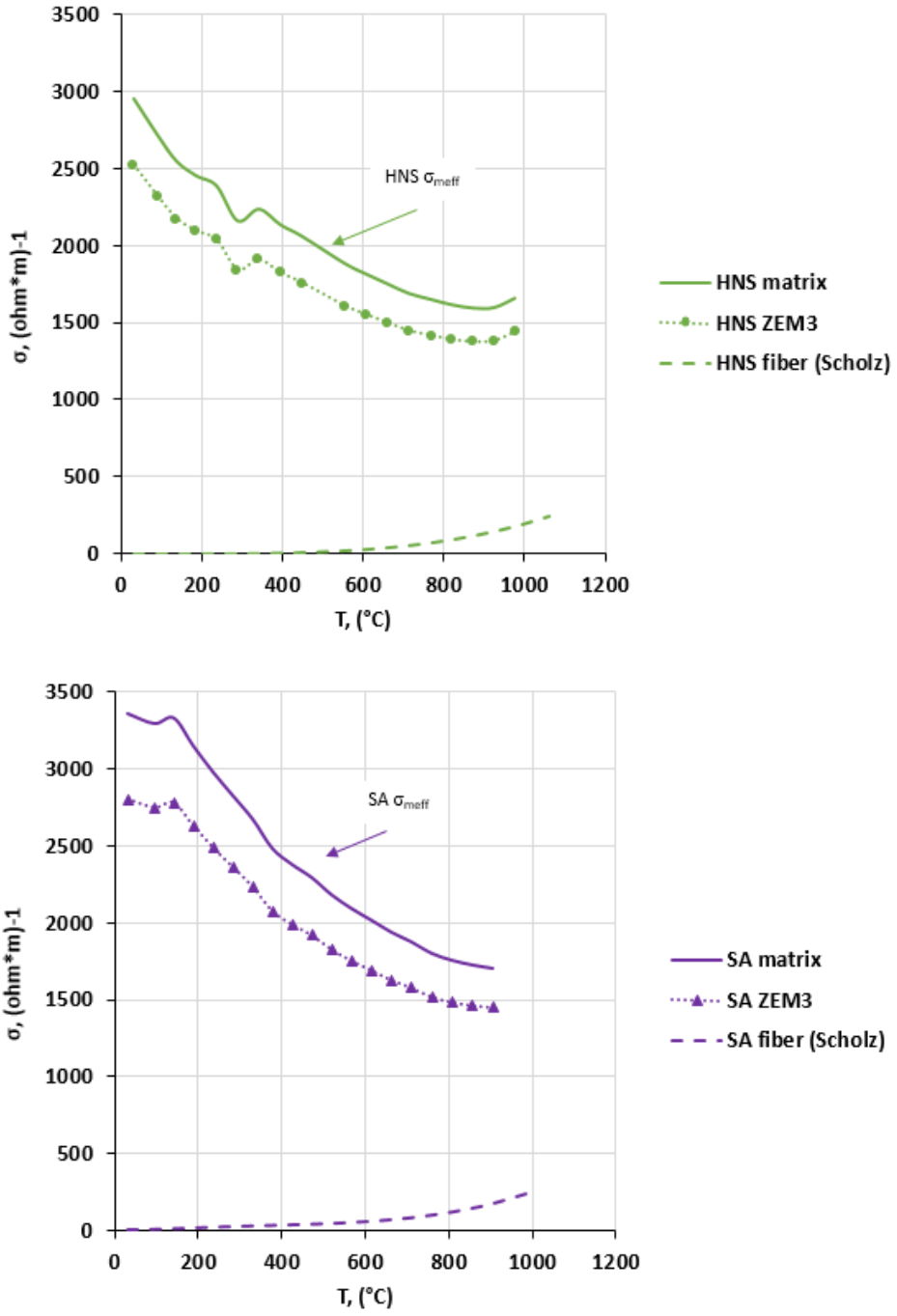

Figure 5.—The calculated electrical conductivity of the effective matrix materials (solid lines) of the (a) HNS and (b) SA reinforced ZEM3 tested samples, respectively. The ZEM3 measured conductivity data (dotted lines) and fiber data (Ref. 7) (dashed lines) used in the parallel circuit.

The results of the parallel circuit model clearly show that the matrix material not only dominates the room temperature electrical conductivity, but continues to dominate with increasing temperature. While the fiber contribution to composite conductivity continues to increase with temperatures, so does the conductivity of the matrix as it transitions into the apparent intrinsic semiconductor region. Therefore, because the matrix is so much more conductive than the fibers across the entire range of temperatures (and continues to increase with temperature), it is believed that the matrix will persist in dominating the electrical response of the composite as it reaches its maximum operating temperature of approximately 1315 °C.

As previously mentioned, the fact that the matrix controls the conductivity of the CMC is the basic principle used in room temperature ER monitoring to correlate change in the resistance to composite damage accumulation via matrix cracking and fiber sliding (Refs. 4 and 5). The results of this simple parallel circuit model confirms that this is also the case at elevated temperature. Therefore, similar damage mechanisms as those described in room temperature tensile tests should also correlate to change in ER during high-temperature thermomechanical testing.

Effect of Thermal Gradient on Overall Electrical Response of Laser-Heated Specimens

Due to the high test temperatures reached in the laser-based heating approach, the inner ER electrodes utilized for recording the temperature-dependent electrical response are placed outside of the laser-heated region (±44.45 mm) near the ends of the tensile bar (±61.2 mm) as shown in Figure 2. While this setup prevents damage to the ER electrodes from high temperature exposure, it means that (unlike the isothermal testing performed in the ZEM3) the resistance recorded during laser testing is a measurement of the heated and non-heated length of the specimen and hence depends on the thermal gradient throughout the specimen. Therefore, it becomes important to understand the role that this thermal gradient has on the overall electrical behavior of the composite during high temperature testing.

The methodology used for determining the temperature distribution along the length of a sample is outlined in Appendix A. For a given hot-zone temperature, the longitudinal thermal gradient in a laser-heated sample is determined by numerical solution of the steady-state heat equation, Equation (12). An investigation of the effect of the thermal gradient on electrical response was performed by examining a ZMI tensile specimen machined from the same panel as the ZMI ZEM3 tested sample was heated using the laser-based approach. This sample (denoted as ZMI-A) is a 6 in. tensile dog-bone specimen with nominal gage cross-sectional dimensions (w x t) of 10.27 mm×4.09 mm (extending to ~12.7 mm width in tab region). Because the ZMI-A tensile specimen was machined from the same panel as the isothermal test specimen, it contains a similar microstructure and likewise similar physical properties. The calculated temperature profiles along the horizontal centerline of the length of ZMI-A from the edge of the heated-region to the end of the sample is shown in Figure 6 for various steady-state values of hot-zone temperature.

The determination of the temperature dependent parameters used in the calculation of the temperature profiles are shown in Figure 8. Heat losses due to thermal radiation were calculated assuming the temperature dependency of emissivity for bulk SiC (Ref. 26), while the temperature dependent values of thermal conductivity were deduced following a linear fit of literature data established for an MI-CVI SiC_f/SiC laminate material (Ref. 2). Finally, the values used for the convection heat transfer coefficient were determined via empirical relationships established for the natural convection from the surface of a horizontal flat plate (Ref. 25). It is worth noting that each profile shown in Figure 6 assumes constant heat transfer properties along the length, based on the given temperature of the heated region. This will of course lead to some inaccuracies in the modeled temperature distributions.

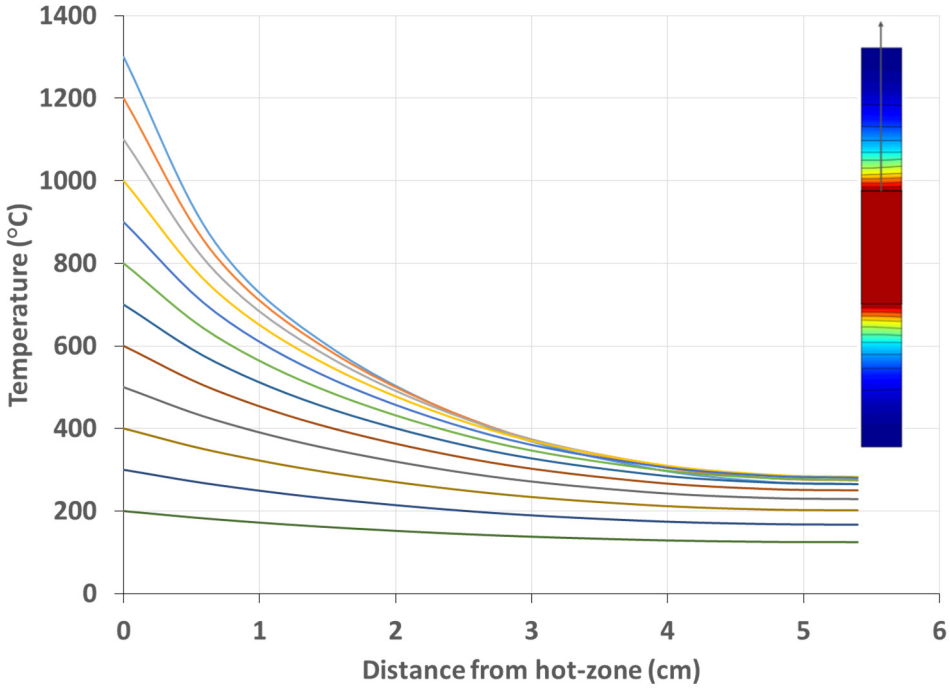

Figure 6.—The calculated longitudinal thermal gradient for the ZMI-A laser-heated sample. Note that each curve represents the temperature profile for a given hot-zone temperature to the end of the tensile specimen.

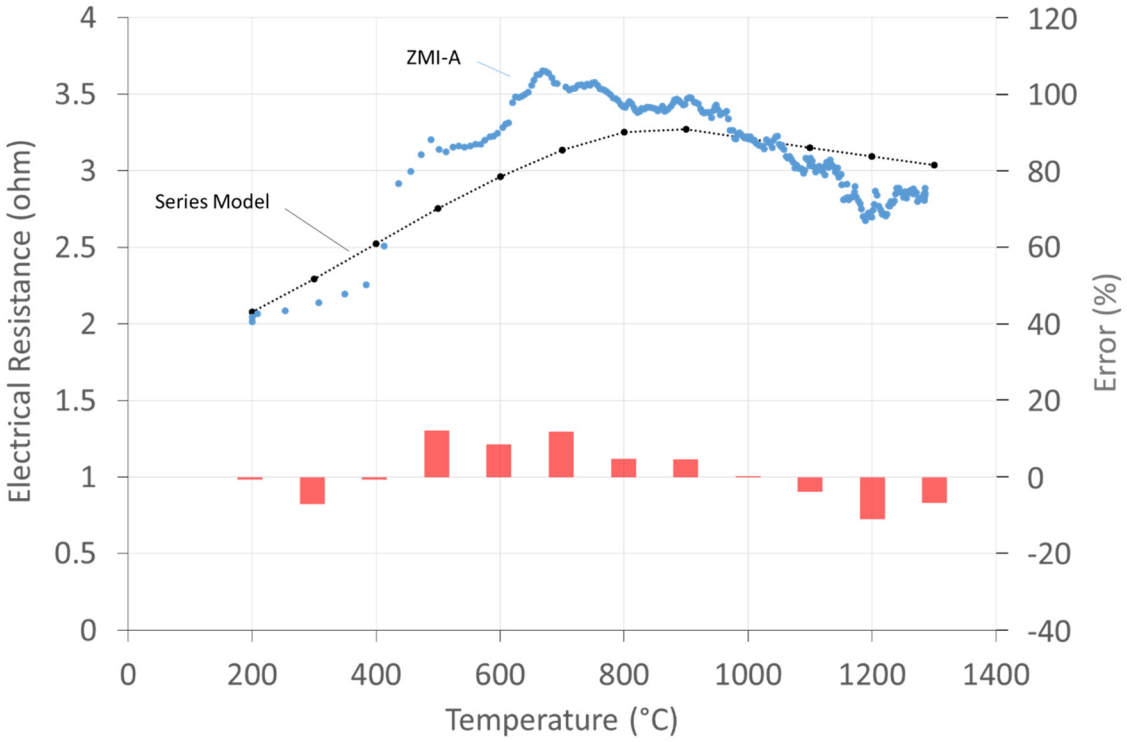

Figure 7.—Comparison of measured electrical resistance to hot-zone temperature of ZMI-A to proposed series resistance model.

Determination of the temperature profile along the length of the specimen can be used in order to model the total resistance of the sample. A simple approximation of the overall resistance of the specimen is done by considering the tensile sample to be a series of distinct elements each assigned a single resistance value, hence the entire sample is modeled as of a series of discrete resistors. By rewriting Equation (1), each resistor in the series can be expressed as a function of the length, cross-sectional area, and temperature-dependent resistivity of the element. Note that by taking a variable cross-sectional area the model is able to account for the change in width from gage to end section of the tensile dog-bone specimen. The total composite resistance can therefore be expressed as the some of these resistance elements as:

$$R_{c\,tot} = \sum R_i = \sum \frac{\rho(T_i)L_i}{A_i} \tag{8}$$

The temperature-dependent resistivity is taken from the experimentally determined isothermal response from the ZEM3 unit. Due to the temperature limitations of the ZEM3 unit, the high temperature response (>900 °C) can be estimated by extrapolating the data following a typical intrinsic semiconductor ($\ln(\rho) \propto 1/T$) relationship. It is worth noting that, due to the large variation in resistivity values between composite samples from different panels, it is necessary to use experimental isothermal data taken from a similar resistivity sample to accurately populate the series model. Therefore, in order to verify the validity of the proposed model, the isothermal ZMI data shown in Figure 1 is extrapolate to 1300 °C and used to model the experimental response of ZMI-A. The modeling results, along with the associated error is shown in Figure 7.

The dashed line representing the results of the model are in general agreement with the experimental data. However, there does appear to be the highest discrepancy across the intermediate hot-zone temperatures (500 to 900 °C). This is likely due to a combination of the relative noise of the signal across these temperatures, as well as the simplifying approximations used in the solution of the temperature profile of the sample. Notably, the use of a constant thermal conductivity and convection coefficient. Furthermore, while the ZEM3 sample used in the model is from the same composite panel as the laser-heated sample, the inhomogeneous nature of MI matrices of these CMCs certainly attributes to some variation of material response.

Conclusions

The present study explores the temperature dependent electrical response of MI-CVI SiC_f/SiC CMCs using both isothermal and laser-based heating approaches. The study examined composite systems containing various reinforcing fiber types, including: Tyranno ZMI and SA, as well as Hi-Nicalon Type S. The novel laser-based setup developed for this study was capable of overcoming the sample size and temperature limitations of typical characterization techniques. Specifically, the laser system was used to heat the gage section of standard tensile coupons used in mechanical testing to temperatures that represent the desired usage temperatures of MI-CVI SiC_f/SiC composites. Therefore, the data collected using this methodology not only provides a unique materials database, but also insight into the possible complexities of extending the use of ER measurements into high temperature thermomechanical tensile testing and damage characterization.

Comparison of the room temperature resistivity of the various test samples represented the wide variation in electrical properties of these materials due to microstructural differences. While sample machined from the same CMC panel appear to have similar resistivity values, samples taken from different panels can vary greatly. For composites containing the same type and relative volume of reinforcing fiber this is presumably caused by variations in matrix microstructure. Specifically, the volume fraction and dispersion of the free silicon remaining in the matrix post melt-infiltration. Clearly, composites containing different fiber types have a combined effect of differences in fiber resistivity and content (however small) as well as these differences in matrix composition. Furthermore, it was found

that exposure to very high test temperatures resulted in a residual increase in the room temperature resistivity of the sample. This finding is significant if ER measurements are to be used to characterize materials that have been exposed to extreme temperatures. That is, knowing the effect of high temperature heat treatment *a prior* is necessary for the deconvolution of a complex ER response.

In terms of temperature dependent behavior, all of the composites tested experienced an initial increase in resistivity with temperature with an observable transition at high temperature. Similar to typical moderately-doped semiconductor behavior, the resistivity increased with temperature up to some transition temperature at which point the resistivity began to decrease. The ability of the laser-based heating setup to achieve temperatures above this transition point allows for a more accurate representation of material behavior in extreme environments. Moving forward, quantification of variations in activation energy and transition temperature could possibly be used to characterize differences in microstructure or impurity concentration.

By considering the composite material as a parallel circuit of continuous phases of SiC fibers and effective matrix material, the contribution of each phase to the overall conductivity of the material was investigated. It was found that the silicon rich siliconized-SiC matrix resulting from the melt-infiltration process dominated the ER of the composite at all temperatures. This finding is extremely important if the use of electrical resistance monitoring is to be extended to damage monitoring of MI-CVI SiC_f/SiC composites under high temperature tensile loading. It has been shown in room temperature uniaxial tension testing of similar materials that because the matrix dominates electrical conduction, that increasing matrix cracking correlates to increasing electrical resistance. Therefore, by demonstrating that the matrix continues to dominate electrical conduction al all temperatures of interest, the same working principle should apply and this type of ER monitoring remains a feasible and cost effective method of damage quantification.

Finally, the significance to overall specimen response of the longitudinal thermal gradient developed using the laser-based heating approach was investigated. One major advantage of this test method is that it can be used to demonstrate the use of ER monitoring in high temperature mechanical testing. However, due to extreme temperatures it becomes necessary to remotely sense the ER response of the gage section. By calculating the temperature profile and using the temperature dependent resistivity data collected using the ZEM3 unit, the contribution of the thermal gradient along the length of the sample to the overall ER response was shown. The approximation of a series circuit resulting in general agreement with experimentally obtain results.

Appendix—Determination of Temperature Profile Using Simplified Heat Transfer Model

In order to calculate the longitudinal thermal gradient generated by the gage-section heating the tensile specimens used in the laser heating approach, various assumptions and boundary conditions need to be defined. First, it should be noted that the sample is relatively thin in comparison to the longitudinal dimension. Therefore, a major simplifying assumption is that the temperature can be assumed relatively constant in the thickness direction. Secondly, because the incident laser energy supplied to the surface of the specimen results in an extremely uniform heating area the temperature of the heated-section is considered constant as well. Since the hot-zone is assumed to be a constant value, a Dirichlet condition (boundary condition of the first kind) is defined along the edges of the heated region. Negligible heat is assumed to be lost through the other edges of the sample (along the sides and top/bottom) and are therefore assigned an insulating Neumann (second kind) boundary condition. Consequently, the resulting convection and radiation losses from the edge of the heated region to the end of the specimen are assumed to be between the faces of the specimen and the surrounding ambient environment. These assumptions simplify the subsequent heat transfer analysis to a 2D approximation of heat losses from the faces of the sample outside the gage section.

The heat transfer from each face of the specimen per unit area do to free convection Q_{conv} can be written as:

$$Q_{conv} = h(T - T_{amb}) \tag{9}$$

where h is a given uniform heat transfer coefficient, T is the temperature at a given location on the sample surface and T_{amb} is the ambient temperature of the surroundings. The heat loss due to radiation per unit area of the front and back specimen faces is defined as:

$$Q_{rad} = \varepsilon\sigma\left(T^4 - T_{amb}^4\right) \tag{10}$$

where ε is the composite surface emissivity and σ is the Stefan-Boltzmann constant. Therefore, the general for of the heat equation can be written as:

$$Dc_p t_c \frac{\partial T}{\partial t} - kt_c\left(\frac{\partial^2 T}{\partial x^2} + \frac{\partial^2 T}{\partial y^2}\right) + 2Q_{conv} + 2Q_{rad} = 0 \tag{11}$$

where the first term represents the time rate of change of thermal energy of the medium in terms of material density D, specific heat c_p and thickness t_c (note that as written this assumes the material is isotropic). However, when there is no change in the amount of energy storage (i.e., steady-state condition) this term goes to zero. The second term represents net conduction along the length of the composite assuming a constant thermal conductivity k, and the final two terms represent the heat losses due to convection and radiation respectively (the factor of two on these terms accounts for the losses of both the front and back faces of the sample). In terms of the steady-state temperature profile, the equation can be rewritten as follows:

$$-kt_c\nabla^2 T + 2hT + 2\varepsilon\sigma T^4 = 2hT_{amb} + 2\varepsilon\sigma T_{amb}^4 \tag{12}$$

Note that because the radiation losses are proportional to temperature to the fourth power, the governing partial differential equation (PDE) shown above is nonlinear. The resulting PDE could be quite difficult to solve analytically because of this nonlinearity and coupling with other modes of energy transfer. Therefore, a numerical approach is often chosen in order to solve for the temperature distribution. Specifically a nonlinear PDE solver based on a damped Newton iteration method was used in order to numerically solve for the temperature field under given material and environmental parameters (Ref. 23).

Establishment of Temperature Dependent Heat Transfer Parameters

Because there is no forced air cooling on the sample, convection heat transfer is driven by the free (natural) convection of warm air ascending from the hot surface of the horizontal samples being replaced by descending cooler fluid from the ambient. The coefficient to be used in calculation of natural convection losses is approximated by considering the buoyancy-driven flow at the surface of the constant heated-region. An average heat transfer coefficient $\bar{h}$ can be expressed in terms of Nusselt number $\overline{Nu_L}$ as:

$$\bar{h} = \frac{k}{L}\overline{Nu_L} \tag{13}$$

where k is the thermal conductivity of the fluid medium (air) and L is the characteristic length of the heated surface. Empirical correlations for external free convection have been determined in which $\overline{Nu_L}$ is expressed in terms of the dimensionless Rayleigh number, Ra_L. A correlation for convection flows from the surface of horizontal flat plates was determined for $Ra_L > 200$ as (Ref. 24):

$$\overline{Nu_L} = 0.59 Ra_L^{1/4} \tag{14}$$

where the Rayleigh number is the product of the Grashof and Prandtl numbers and is defined as:

$$Ra_L = \frac{g\beta(T_{sur} - T_\infty)L^3}{\nu\alpha} \tag{15}$$

where T_{sur} and T_∞ are the surface and ambient temperatures respectively, g is the acceleration due to gravity, and β, ν and α are thermal expansion coefficient, kinematic viscosity and thermal diffusivity of air evaluated at the film temperature, $T_f = (T_{sur} + T_\infty)/2$. It has been shown that improved accuracy of these correlations can be obtained by considering the form of the characteristic length as the ratio (Ref. 24):

$$L = \frac{A_S}{P} \tag{16}$$

where A_s and P are the plate surface area and perimeter, respectively. Therefore, by using the thermophysical properties of air at ambient pressure (Ref. 25) and the characteristic length of a nominal tensile specimen with surface dimensions of 152.4×12.7 mm, it is possible to estimate the free convection coefficient of a horizontal sample as a function of surface temperature by the solution of Equation (13) in terms of Equations (14) to (16). Results of this analysis are plotted in Figure 8 for 200 °C < T_{sur} < 1300 °C. Note that the use of this correlation will lead to a slight overestimation of the convection losses. This is due to the fact that Equation (14) was established from empirical data found for a constant temperature (isothermal) plate, whereas our sample experiences a temperature drop outside the constant temperature heated section.

The solution of Equation (12) also requires knowledge of the temperature dependent emissivity of the sample. It is known that semiconductive materials have relatively high emissivity values, and literature data on the temperature dependence of SiC is readily available (Ref. 26). The emissivity values used in analysis are shown in Figure 8. While emissivity depends on the nature of the surface and sample microstructure, this should be a reasonable approximation for the purposes of this study.

Finally, it is necessary to establish the temperature dependence of the thermal conductivity to be used in the solution of the heat equation. In-plane thermal conductivity data for SiC_f/SiC composites has been reported for both room and high temperature (1200 °C) (Ref. 2). A linear fit to these engineering estimates has been produced and is shown in Figure 8. This trend should be a responsible estimate as the data refers to similar slurry melt-infiltrated SiC_f/SiC composites. Furthermore, this data was established for in-plane data as opposed to the more commonly reported transverse conductivity.

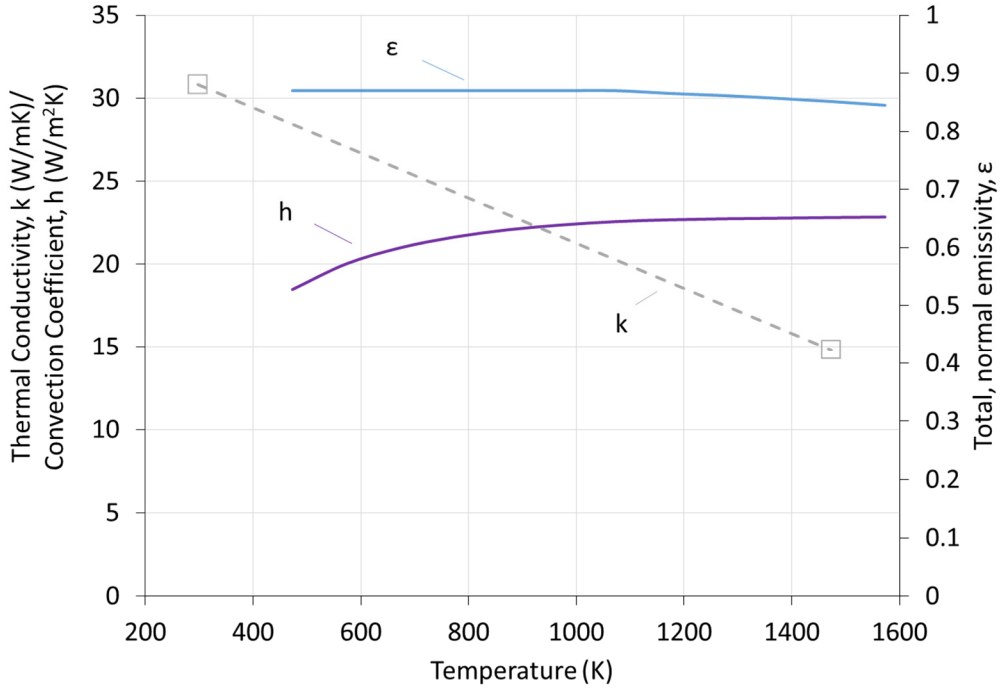

Figure 8.—Temperature dependencies of thermal conductivity (k), natural convection coefficient (h), and emissivity (ε) used in the numerical solution of longitudinal thermal gradient.

References

1. Dicarlo J.A., Yun H-M., Morscher G.N., et al. SiC/SiC Composites for 1200C and Above. In: Handbook of Ceramic Composites. 2005, pp. 77–98.
2. Corman G.S., Luthra K.L., Silicon Melt Infiltrated Ceramic Composites (HiPerComp). In: Handbook of Ceramic Composites. 2005, pp. 99–115.
3. Dicarlo J.A., Advances in SiC/SiC Composites for Aero-Propulsion. In: Ceramic Matrix Composites: Materials, Modeling and Technology. 2015, pp. 217–235.
4. Smith C., Morscher G., Xia Z., Monitoring damage accumulation in ceramic matrix composites using electrical resistivity. Scr Mater; 59: 463–466.
5. Morscher G.N., Baker C., Smith C., Electrical Resistance of SiC Fiber Reinforced SiC/Si Matrix Composites at Room Temperature during Tensile Testing. Int J Appl Ceram Technol; 11: 263–272.
6. Appleby M., Morscher G.N., Zhu D. Creep and Environmental Durability of Environmental Barrier Coatings and Ceramic Matrix Composites under Imposed Thermal Gradient Conditions. In: ICACC 37 Conference Proceedings 2013. 2013.
7. Scholz R., Santos F., Riccardi B., Electrical conductivity of silicon carbide composites and fibers. J Nucl Mater; 307: 1098–1101.
8. Youngblood G.E., Thomsen E, Shinavski R. Electrical Conductivity of 2D-SiCf/CVI-SiC. Fusion Sci Technol an Int J Am Nucl Soc; 60: 364–368.
9. North B., Gilchrist K.E., Effect of Impurity Doping on a Reaction Bonded Silicon Carbide. Am Ceram Soc Bull; 60: 549–555.
10. ULVAC Website Available at http://www.ulvac.com/oem/index.cfm
11. Morscher G.N., Pujar V.V., Design Guidelines for In-Plane Mechanical Properties of SiC Fiber-Reinforced Melt-Infiltrated SiC Composites. Int J Appl Ceram Technol; 6: 151–163.
12. Zhu D., Miller R.A., Nagaraj B.A., et al. Thermal conductivity of EB-PVD thermal barrier coatings evaluated by a steady-state laser heat flux technique. Surf Coatings Technol; 138: 1–8.

13. Zhan G-D, Mitomo M., Mukherjee A.K., Effects of heat treatment and sintering additives on thermal conductivity and electrical resistivity in fine-grained SiC ceramics. J Mater Res; 17: 2327–2333.
14. Roewer G., Herzog U., Trommer K, et al. Silicon Carbide - A Survey of Synthetic Approaches , Properties and Applications. In: High Performance Non-oxide Ceramics I. 2002, pp. 59–135.
15. Abderrazak H., Hmida ESBH. Silicon Carbide: Synthesis and Properties. In: Properties and Applications of Silicon Carbide, pp. 361–389.
16. Inoue K., Mori S., Yamaguchi A., Thermal Conductivity and Temperature Dependence of Electrical Resistivity of Al 4 SiC 4 SiC Sintered Bodies Prepared by Pulse Electronic Current Sintering. J Ceram Soc Japan; 111: 466–470.
17. Smith C.E., Morscher G.N., Xia Z. Electrical Resistance as a Nondestructive Evaluation Technique for SiC/SiC Ceramic Matrix Composites Under Creep-Rupture Loading. Int J Appl Ceram Technol; 8: 298–307.
18. Racette J.H., Intrinsic Electrical Conductivity in Silicon Carbide. Phys Rev; 107: 1542–1544.
19. Yacobi B.G., Semiconductor Materials: An Introduction to Basic Principles, Springer Science & Business Media, 2003.
20. Yu PY, Fundamentals of Semiconductors: Physics and Material Properties, Springer, 1996.
21. Bhatt R., Chen Y.L., Heat Treatment Effects on Microstructure of SiC Fiber Preforms. NASA TM 1999; 209292.
22. Orlova T.S., Popov V.V., Quispe Cancapa J, et al. Electrical properties of biomorphic SiC ceramics and SiC/Si composites fabricated from medium density fiberboard. J Eur Ceram Soc; 31: 1317–1323.
23. http://www.mathworks.com/help/pde/ug/nonlinear-equations.html
24. Goldstein R.J., Sparrow EM, Jones DC. Natural Convection Mass Transfer Adjacent to Horizontal Plates. Int J Heat Mass Transf; 16: 1025–1035.
25. Incropera Frank P., DeWitt David P., Introduction to Heat Transfer 3rd ed., Wiley & Sons, 1996.
26. Touloukian Y.S., DeWitt P.D. Thermal radiative properties: nonmetallic solids. Thermophys Prop Matter, Vol 8 1972.
27. Mackey J., Dynys F., Sehirlioglu A. Uncertainty analysis for common Seebeck and electrical resistivity measurement systems. Rev Sci Instrum; 85: 085119.